# Quantification of cardiac fiber orientation using optical coherence tomography

**Christine P. Fleming,a, Crystal M. Ripplinger,b Bryan Webb,a Igor R. Efimov,b and Andrew M. Rollinsa**

aCase Western Reserve University, Biomedical Engineering Department, 10900 Euclid Avenue, Cleveland, Ohio 44106
bWashington University in St. Louis, Biomedical Engineering Department, One Brookings Drive, St. Louis, Missouri 63130

**Abstract.** Heterogeneity in cardiac tissue microstructure is a potential mechanism for the generation and maintenance of arrhythmias. Abnormal changes in fiber orientation increase the likelihood of arrhythmia. We present optical coherence tomography (OCT) as a method to image myofibers in excised intact heart preparations. Three-dimensional (3-D) image sets were gathered from the rabbit right ventricular free wall (RVFW) using a microscope-integrated OCT system. An automated algorithm for fiber orientation quantification in the plane parallel to the wall surface was developed. The algorithm was validated by comparison with manual measurements. Quantifying fiber orientation in the plane parallel to the wall surface from OCT images can be used to help understand the conduction system of the specific sample being imaged. © *2008 Society of Photo-Optical Instrumentation Engineers.* [DOI: 10.1117/1.2937470]

## 1 Introduction

Proper action potential conduction through the heart are required for normal heart function. Fiber orientation, the alignment of myocytes within the heart wall, greatly influences wavefront propagation. Therefore, abnormal fiber orientation increases the likelihood of abnormal cardiac rhythms, or arrhythmias.[1]

Current methods for measuring fiber orientation range from histology[2,3] to diffusion tensor magnetic resonance imaging.[4] It is known that fiber angle varies in a nearly linear fashion from the epicardium to the endocardium.[2,3] Karlon and colleagues developed an automated image analysis method for measuring fiber orientation from histology slices.[5] The method uses intensity based gradients within an image to calculate fiber orientation and angular standard deviation.

Optical coherence tomography (OCT) is a nondestructive, noncontact imaging modality that can generate 3-D images rapidly with high spatial resolution.[6] OCT detects minimally

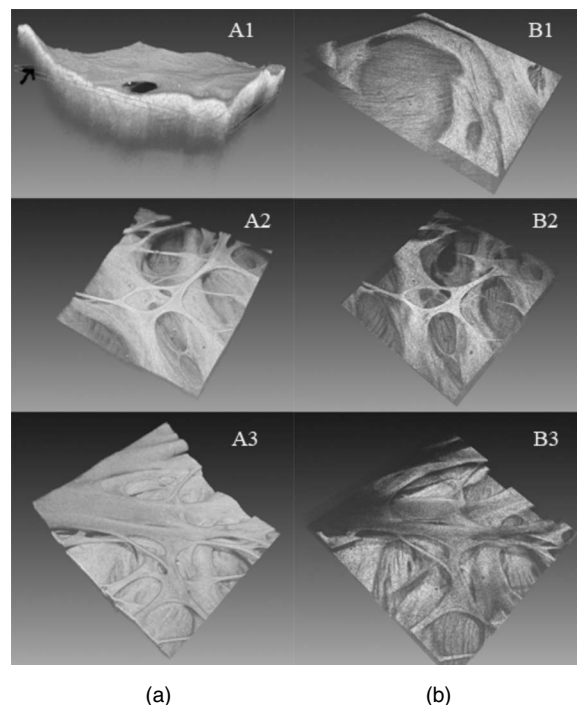Tel: (216) 368–1684; E-mail: cfleming@case.edu



**Fig. 1** 3-D OCT data sets of the right ventricular free wall (RVFW). (a) 3-D OCT images of the RVFW, data sets (a1) RVFW1, (a2) RVFW2, and (a3) RVFW3. The arrow in A1 points to cross-sectional (*en face*) slices. (b) View of three *en face* slices in depth within the 3-D OCT data sets. The fiber structure is visible within the *en face* slices. The uneven sample surface (b1) and trabeculations [(b2) and (b3)] induce low-frequency changes and produce shadows within subsequent *en face* slices, inducing a gradient that may be greater than the gradient produced by the fibers.

scattered light and utilizes intrinsic scattering contrast within samples to generate an image. OCT is capable of imaging to depths of 1 to 2 mm in cardiac tissue.[7–9] In this letter, we present and validate an automated method for quantifying fiber orientation from structurally intact excised cardiac tissue preparations using intensity-based gradients applied to OCT *en face* images.

## 2 Methods

Three-dimensional OCT image sets of the endocardial surface of an isolated right ventricular free wall (RVFW) preparation from a New Zealand white rabbit were used in this study. The protocol was approved by the Institutional Animal Care and Use Committee at Washington University. The experimental procedures have been previously described.[10] The RVFW was dissected, stretched, and pinned epicardial side down onto a silicon disk. The sample was placed in 3.7% formaldehyde for one day and 20% sucrose solution for an additional two days. This dehydration step improves the visibility of the fibers under OCT imaging.

A microscope-based OCT system[11] was used to image volumes of the sample. The axial and lateral resolution of the system was approximately 10 $\mu$m (in air). The three data sets presented in this work vary in structural complexity [Fig. 1(a)]. Each volume was 4.5 mm $\times$ 4.5 mm $\times$ 3.16 mm, corresponding to a pixel size of 11.25 $\mu$m $\times$ 11.25 $\mu$m
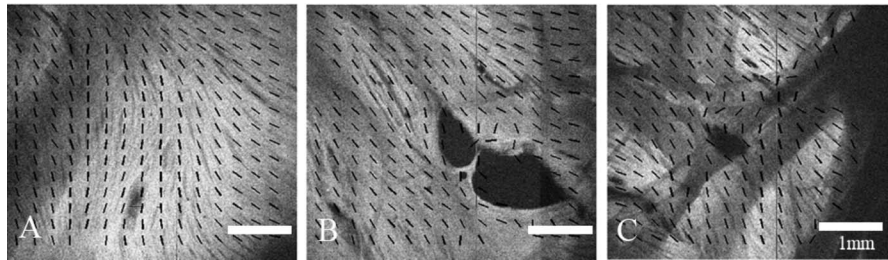
**Fig. 2** Fiber orientation in the rabbit right ventricle. An automated algorithm enables quantification of the fiber orientation in the plane parallel to the wall surface for samples of varying structural complexities: (a) RVFW1, (b) RVFW2, and (c) RVFW3. Although there are gradients within the images due to uneven surfaces (a) and shadows created by trabeculations [(b) and (c)] the two-step filtering process effectively reduce their contribution to the gradient magnitude calculations.

$\times 4.86$ $\mu$m. To calculate fiber orientation from 2-D OCT images, a modification of the intensity-based gradient algorithm described by Karlon et al.[5] was used.

Within *en face* OCT images [Fig. 1(b)], uneven sample surface topology (e.g., RVFW1) and shadows cast by trabeculations (e.g., RVFW2 and RVFW3) cause low spatial frequency changes in the background intensity. These artifacts introduce unwanted intensity gradients within the image. A 2-D second-order Butterworth high-pass filter was used under the assumption that the surface topology and shadowing artifacts have lower spatial frequency components compared to visible fiber structures. The high-pass filter was convolved with the *en face* OCT image to suppress variations in background intensity. The high-pass filtered *en face* OCT image was convolved with a Wiener filter for noise reduction.

Two-dimensional $3 \times 3$ Sobel filters were used to estimate local gradients in the image. $G_x$ and $G_y$ are defined as the convolution of the horizontal and vertical Sobel filters with the 2-D *en face* filtered OCT images. For each pixel, the magnitude of the gradient, $G(i,j)=(G_x^2+G_y^2)^{1/2}$ and the gradient direction, $\theta'=\text{atan}(G_y/G_x)$, was calculated.

Within a small local window of the image, $W$, the dominant local direction of the gradient was computed by taking the maximum of the angular distribution function, $A_\theta^W$, a function of $G(i,j)$ and $\theta'(i,j)$, as described by Karlon et al.[5] The angular distribution function is a fit of a radial normal distribution to the distribution of angles within the local window.

The directions of the cardiac fibers were assigned as perpendicular to the direction of the dominant local gradients. Two criteria were used to reject invalid fiber orientation assignments. First, the algorithm identified windows with no tissue present by using a threshold on the average pixel intensity within the window. Second, to measure the confidence in fiber orientation measurements produced by the automated algorithm, a D'Agostino-Pearson $\kappa^2$ (normality) test was conducted on the angular distribution of calculated orientations within each window. High values of $\kappa^2$ indicate that the angular distribution function is not a normal distribution, and therefore, the confidence in the fiber orientation assignment in that window is low. Threshold values for $\kappa^2$ (0.02) and average intensity values within a window (80, 1.5 times the noise floor) were selected. The automated algorithm was implemented using the software package MATLAB 7.3.0.267 R2006b (© 1984–2006, The Mathworks, Inc.).

In order to validate the method quantitatively, an investigator blinded to the results of the automated algorithm manually measured fiber orientation angles on the *en face* OCT images analyzed by the automated algorithm. *En face* images
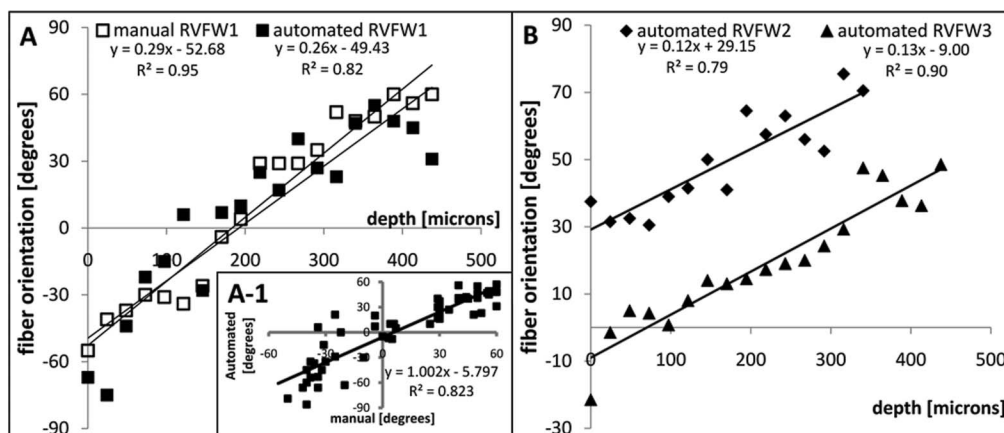


**Fig. 3** Fiber orientation as a function of depth. (a) Fiber orientation as a function of depth for RVFW1 comparing automated (solid squares) and manual (open squares) measurements for a $281 \times 281 \times 500$ $\mu$m volume. (a1) Comparison of fiber orientation measurements for an $1125 \times 1125 \times 500$ $\mu$m volume within RVFW1. Open squares—RVFW1 manual; solid squares—RVFW1 automated. The automated fiber orientation measurements agree very well with the manual fiber orientation measurements. (b) Fiber orientation as a function of depth for RVFW2 (solid diamonds) and RVFW3 (solid triangles) for a $281 \times 281 \times 500$ $\mu$m volume. The fiber orientation changes monotonically with depth.

were analyzed in increments of 25 $\mu$m in depth for all three data sets. Results from the automated algorithm were compared to manual measurements by analyzing the mean and standard deviation of fiber orientation assignments for each depth and orientation as a function of depth. This comparison was made using several window sizes, but the mean of the absolute difference was the lowest for a window size of 563 $\mu$m $\times$ 563 $\mu$m (almost four myocytes in length, assuming that an adult cardiac myocyte has an average length of 150 $\mu$m). Results using a 563 $\mu$m $\times$ 563 $\mu$m window were resampled to obtain 256 vectors per image. Under these settings, the 2-D fiber orientation algorithm runs in less than 7 s per image using a Workstation with an Intel processor running at 2.66 GHz and 2-GB SDRAM memory, 533 MHz with Windows.

## 3 Results

Accurate fiber orientation measurements were obtained from all three data sets up to 500 $\mu$m below the sample surface. Figure 2 shows example vector plots of fiber orientations overlaid on raw *en face* OCT images. The low-frequency background intensity change and shadows created by endocardial trabeculations are apparent within the raw OCT image. Preprocessing of the data effectively reduced the gradient contribution of these features, producing accurate measurements of fiber orientation for samples of varying structural complexity.

It has been well established that normal fiber orientation varies nearly monotonically from the epicardium to the endocardium. Figure 3 shows fiber orientation measurements as a function of depth for representative 281 $\mu$m $\times$ 281 $\mu$m $\times$ 500 $\mu$m volumes from each of the three data sets. In all three cases, there is a nearly linear change in fiber orientation with depth. Comparing the slopes for the RVFW1 volume shows that the automated measurements correspond very well to the manual measurements [Fig. 3(a)]. A quantitative comparison of fiber orientation assignments was conducted on an 1125 $\times$ 1125 $\times$ 500 $\mu$m volume randomly selected within the RVFW1 data set [Fig. 3(a)]. Fiber orientation assignments made by the automated algorithm correlated very well to manual measurements, with a 1.002 slope and a 0.823 correlation coefficient.

## 4 Discussion and Conclusion

In summary, an automated algorithm was developed and validated for quantifying cardiac fiber orientation within OCT image sets. During this study, the sample surface was made relatively flat through the use of pins, and dehydration agents enhanced the visibility of fibers in OCT image sets. These are procedures that cannot translate directly to *in vivo* imaging. Therefore, developing an OCT scanner with high axial and transverse resolution may alleviate the need for dehydration and fixation protocols. Maintaining a relatively constant transverse resolution with depth will increase the visibility of fibers in depth. In addition, there is a need to extend this algorithm to quantify fiber orientation in three dimensions to accommodate samples with irregular fiber orientation patterns and samples with curved surfaces. Quantifying fiber orientation in structurally intact excised preparations using OCT can potentially be used to correlate fiber orientation with electrical conduction properties (e.g., conduction velocity) and mechanical properties (e.g., strain analyses) of the myocardium in a variety of heart disease and arrhythmia models.

### References

1. A. Kleber and Y. Rudy, "Basic mechanisms of cardiac impulse propagation and associated arrhythmias," *Physiol. Rev.* **84**, 431–488 (2004).
2. D. D. Streeter, H. M. Spotnitz, D. J. Patel, J. J. Ross, and E. H. Sonnenblick, "Fiber orientation in the canine left ventricle during diastole and systole," *Circ. Res.* **24**, 339–347 (1969).
3. D. D. Streeter, R. N. Vaishnav, D. J. Patel, H. M. Spotnitz, J. J. Ross, and E. H. Sonnenblick, "Stress distribution in the canine left ventricle during diastole and systole," *Biophys. J.* **10**(4), 345–363 (1970).
4. P. Helm, M. Beg, M. Miller, and R. Winslow, "Measuring and mapping cardiac fiber and laminar architecture using diffusion tensor MR imaging," *Ann. N.Y. Acad. Sci.* **1047**, 296–307 (2005).
5. W. J. Karlon, J. W. Covell, A. D. McCulloch, J. J. Hunter, and J. H. Omens, "Automated measurement of myofiber disarray in transgenic mice with ventricular expression of ras," *Anat. Rec.* **252**, 612–625 (1998).
6. B. E. Bouma and G. J. Tearney, Eds., *Handbook of Optical Coherence Tomography*, Marcel Dekker, Inc., New York (2002).
7. M. W. Jenkins, R. S. Wade, Y. Cheng, A. M. Rollins, and I. R. Efimov, "Optical coherence tomography imaging of the purkinje network, *J. Cardiovasc. Electrophysiol.* **16**(5), 559–560 (2005).
8. C. Sun, Y. Wang, L. Lu, C. Lu, I. Hsu, M. Tsai, C. Yang, Y. Kiang and C. Wu, "Myocardial tissue characterization based on a polarization-sensitive optical coherence tomography system with an ultrashort pulsed laser," *J. Biomed. Opt.* **11**(5), 054016 (2006).
9. M. Jenkins, O. Chughtai, A. Basavanhally, M. Watanabe, and A. Rollins, "*In vivo* gated 4-D imaging of the embryonic heart using optical coherence tomography," *J. Biomed. Opt.* **12**(3), 030505 (2007).
10. C. M. Ripplinger, V. I. Krinsky, V. P. Nikolski, and I. R. Efimov, "Mechanisms of unpinning and termination of ventricular tachycardia," *Am. J. Physiol. Heart Circ. Physiol.* **291**, H184–H192 (2006).
11. Z. Hu and A. M. Rollins, "Quasi-telecentric optical design of a microscope-compatible OCT scanner," *Opt. Express* **13**(17), 6407–6415 (2005).